Macromolecules

pubs.acs.org/Macromolecules Article

Dynamics of DNA-Bridged Dumbbells in Concentrated, Shear-Banding Polymer Solutions

Seunghwan Shin, Yangming Kou, Kevin D. Dorfman,* and Xiang Cheng*

Cite This: *Macromolecules* 2021, 54, 4186−4197 Read Online

ACCESS | Metrics & More | Article Recommendations | Supporting Information

ABSTRACT: Although experimental evidence for shear-banding flows in concentrated polymer solutions has accumulated over the last 20 years, the origin of such shear-banding flows is still under heated debate. Experiments that probe the microscopic dynamics of shear-banding polymer solutions are still scarce. Here, using a custom-built high-resolution rheo-confocal shear cell, we experimentally study the dynamics of DNA-bridged colloidal dumbbells in the shear-banding flow of concentrated double-stranded DNA (dsDNA) solutions under large amplitude oscillatory shear. We synthesize dumbbells consisting of two spherical colloids linked by λ-DNA and track their 2D-projected configurations in sheared dsDNA solutions. We first confirm that the velocity profile of the concentrated dsDNA solutions is inhomogeneous at high Weissenberg numbers and exhibits strong shear banding with two distinct shear bands. We then measure the orientational distribution of the DNA-bridged dumbbells and investigate their translational and rotational dynamics within the two shear bands. The preferred alignment of the dumbbells along the flow direction in the high-shear-rate band suggests the dominant role of elastic stresses in that band. In contrast, a bimodal distribution of dumbbell orientations is observed in the low-shear-rate band, indicating more balanced contributions from both normal and elastic stresses. Furthermore, exclusively in the high-shear-rate band, we also find spatially localized correlated enhanced translational and rotational motions and a strong coupling between enhanced translation and chain extension. These unique conformational and dynamic features suggest shear-induced breakage of the local entanglement network in the high-shear band, which we postulate leads to puddles of low viscosity within an otherwise high-viscosity fluid. Together, our quantitative analyses of the spatially distinct dynamics of dsDNA-bridged dumbbells in coexisting shear bands provide important insights into the microscopic origin of shear-banding flows in concentrated polymer solutions.

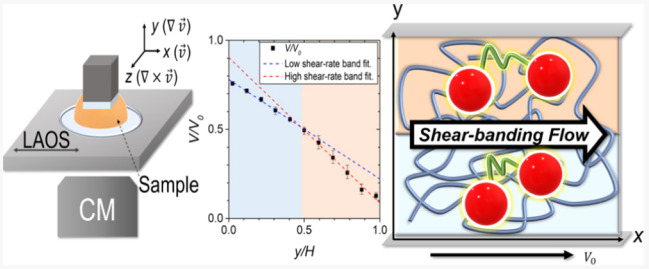

1. INTRODUCTION

Shear banding, a heterogeneous shear profile with spontaneously separated domains of different shear rates, is observed in a variety of complex fluids undergoing strong shear flows.[1−4] Its emergence in concentrated polymer solutions and melts was theoretically predicted long ago using the Doi−Edwards original tube model[5] and first experimentally reported more than 20 years ago.[6,7] Experimental evidence in support of the existence of shear banding in polymer solutions has since accumulated in different polymer systems under different shear protocols including time-independent steady shear and time-dependent start-up and oscillatory shear.[8−14] Despite the extensive research efforts in recent years, the microscopic origin of shear banding in polymer solutions remains controversial.[15] Although several scenarios have been proposed to account for this nonlinear flow feature including strong flow-concentration coupling,[16−19] shear-induced localized disentanglement of networks,[20,21] instabilities triggered by stress overshoot,[22−24] and long-penetrating edge disturbances,[25,26] benchmark experiments that can reveal the microscopic dynamics of shear-banding polymer solutions and verify the assumptions and predictions of these competing theories are still missing.

Worm-like micelles are probably the best studied polymeric system exhibiting shear banding.[27,28] They can aggregate into long cylindrical filaments entangled with each other to form transient entanglement networks, analogous to entangled polymer networks. Experiments using flow birefringence, NMR, and SANS showed that the entangled filaments display strong alignment along the flow direction in the high-shear-rate band (SRB).[29−32] Such a finding suggests that the shear-induced conformation and dynamics of polymer chains are the key to understand the origin of shear banding in concentrated polymer solutions. To probe shear-induced chain dynamics, single molecule level visualization of polymer chains in the sea

Received: December 31, 2020
Revised: April 5, 2021
Published: April 20, 2021

https://doi.org/10.1021/acs.macromol.0c02890
Macromolecules 2021, 54, 4186−4197

of unlabeled background polymers has been conducted. Most of these studies adopted double-stranded DNA (dsDNA) thanks to its micron-scale size, semiflexible nature, and ease of labeling with bright bisintercalating dyes such as YOYO-1.[33−37] However, this approach is limited to the dilute/semidilute regime in relatively slow flows due to the weak fluorescence signal associated with individual molecules, which is far from sufficient for imaging in the fast flows of highly concentrated solutions necessary for the development of shear banding. Alternatively, direct observations of F-actin filaments in nonlinear flows have also been achieved.[12,38] Nevertheless, these filaments are qualitatively different from typical flexible polymers, in that their persistence length is comparable to or even longer than their contour length.

Here, we propose a new approach to probe chain level dynamics in the shear-banding flow of concentrated polymer solutions. To overcome the experimental difficulty in imaging single DNA molecules in highly concentrated solutions, we synthesize dumbbells of fluorescent colloids linked by long linear DNA molecules. While the brightness of the colloidal particles allows for high-speed imaging in fast flows of concentrated DNA solutions, the bridging linear DNA linkers provide insights into the conformation and dynamics of entangled chains in the sheared samples. Specifically, we use a custom planar Couette confocal shear cell to observe the dynamics of DNA-bridged dumbbells in the flow−vorticity plane. By tracking the conformation and position of DNA-bridged dumbbells over time, we observe spatially distinct dumbbell dynamics in the two coexisting shear bands. In the high-SRB, we find a pronounced alignment of dumbbells along the flow direction, drastically enhanced translational and rotational dynamics, and strong couplings between translation and rotation and between translation and chain extension. Such spatially distinct dumbbell dynamics shed new light onto the microscopic origin of shear banding in concentrated polymer solutions and provide important insights into the dynamics of polymer chains in shear-banding flows. We conclude by discussing the implication of our experimental findings for existing shear-banding theories.[16−18,21,23,25,39−43]

2. MATERIALS AND METHODS

2.1. Synthesis of DNA-Bridged Colloidal Dumbbells. Synthesis of DNA-bridged colloidal dumbbells consists of three major steps. A connecting DNA linker was first prepared. Reactive antigens were then introduced to the surface of colloidal particles in a separate reaction. Finally, the synthesized DNA linkers and the surface-modified particles were mixed together for a bridging reaction. In the following sections, we describe the general steps of the synthesis. Interested readers are encouraged to refer to the Supporting Information for more details.

2.1.1. Synthesis of DNA Linkers. DNA linkers were prepared by ligating the sticky ends of a long linear dsDNA with complementary single strands that contain reactive groups [biotin or digoxygenin (DIG)] at their 3′-ends. In our study, λ-DNA was used as long linear DNA linkers (New England Biolabs, 48.5 kbp) with both chain ends single-stranded. These reactive sticky ends were hybridized with excess amounts of oligomers of the two types (biotin or DIG) (Integrated DNA Technologies), each of which has a complementary base pair sequence to the corresponding sticky end. The hybridized dsDNA linkers had nicks in their phosphate backbones, which were repaired by a standard ligation step. The unbound oligomers were removed by gel electrophoresis (Owl EasyCast B1 Mini Gel Electrophoresis Systems, Thermo Fisher Scientific), while the ligated product was recovered by gel digestion. To remove residual agarose and enzymes from the reaction mixture after the gel digestion, the reaction mixture was purified by drop dialysis using a disc filter (MilliporeSigma) floating on 1× TBE buffer. The DNA concentration was measured using a UV−vis spectrometer (NanoDrop) and then diluted with 1× TBE buffer to achieve a final concentration of 10 μg/mL or 0.33 nM. Successfully ligated DNA linkers had biotin at one end and DIG at the other end.

2.1.2. Surface Modification of Colloidal Particles. Fluorescent carboxylated magnetic polystyrene (PS) particles of diameter d = 2.9 μm were acquired from Bangs Laboratories. The particles were functionalized with either streptavidin or anti-DIG and then passivated by methoxypoly(ethylene) glycol amine (mPEG-NH_2, M_w = 5000, Alfa Aesar) via 1-ethyl-3-(3-dimethylaminopropyl) carbodiimide hydrochloride (EDC)/NHS coupling. The particle coating protocol was modified based on a previous study.[44] The particles were initially dispersed in MES buffer. EDC and *N*-hydroxysulfosuccinimide sodium salt (Sulfo-NHS) were sequentially added to the particle suspension while stirred on a vortex mixer for the activation of the carboxylic groups on the particle surface. Then, the activated particles were washed and resuspended in PBS buffer (phosphate-buffered saline, 137 mM NaCl, 2.7 mM KCl, 10 mM Na_2HPO_4, 1.8 mM KH_2PO_4, with a pH of 7.4), which was followed by the addition of either streptavidin or anti-DIG. After a reaction of 4 h, mPEG-NH_2 dissolved in 200 μL of 1× PBS buffer was added to the reaction mixture for passivation of the particles. After the reaction was allowed to continue for additional 40 h, it was quenched by adding glycine. The resulting conjugated particles were finally washed and suspended in 1× TBE buffer.

2.1.3. Synthesis of DNA-Bridged Dumbbells. The rate of reaction between DNA linkers and colloid particles in solution is limited by the Brownian diffusion of the particles, which brings particles into close proximity for DNA bridging. To facilitate the linking reaction, we constructed a reactor following a previous study.[45] Figure 1 shows a schematic of our reactor, which was 3D printed in polyacrylonitrile and has a rectangular well with a small opening sealed by a glass coverslip at the center for microscopy. A 50:50 mixture of streptavidin-coated and anti-DIG-coated particles was injected into the well, followed by the addition of the ligated DNA linker solution. Due to the high specific gravity of the magnetic particles relative to the solvent, they quickly sedimented down to the bottom. The reactor was put inside a closed Petri dish chamber with a solvent trap to reduce solvent evaporation and a horseshoe magnet of about 80 G was placed on top of the lid, which aligned the particles into long strings with close contacts. After overnight reaction, the magnet was removed and the sample solution was recovered by gently aspirating with a wide-mouthed pipette.

During the reaction, the two types of particles, that is, streptavidin-coated and anti-DIG-coated particles, are brought into long, stable strings by the magnetic field with random sequences (Figure 1a). Biotin/streptavidin and DIG/anti-DIG interactions are highly selective. Thus, a DNA linker capped by biotin and DIG at each end cannot form a closed loop on the same particle. A bridge can form only between sequential neighbors of different types along a string. Note that, as the size of a particle is larger than the radius of gyration of λ-DNA (0.58 μm[35]), it is unlikely that a linker forms a bridge between distant particles. Even though we cannot completely prevent the formation of colloidal chains of more than two particles, the probability of forming long chains decays rapidly with their lengths. Consequently, the majority of the particles in our suspensions after the reaction are in the form of either monomers or dimers (Figure 1b right). In addition to the successfully linked DNA chains between two particles, the surfaces of the particles are also covered by grafted DNA molecules with one free end. By entangling with background DNA in concentrated DNA solutions, these grafted DNA chains reduce the degree of slippage on particle surfaces. Once the DNA-bridged dumbbells were synthesized, they were dispersed in 1× TBE buffer.

We conducted control experiments to verify our synthetic method (Figure 1b). To confirm selective antibody/antigen interactions and the protection of particles from nonspecific attraction, we added the YOYO-1 fluorescent intercalating dye to the ligated λ-DNA and let it

https://doi.org/10.1021/acs.macromol.0c02890
Macromolecules 2021, 54, 4186−4197

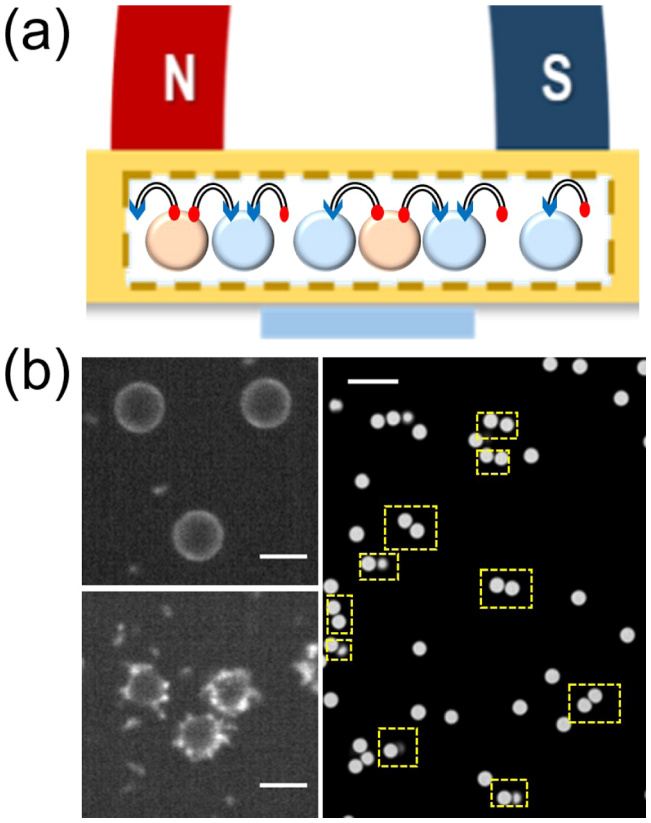

Figure 1. Synthesis of DNA-bridged colloidal dumbbells. (a) Schematic showing the reactor for the synthesis. The well at the center of the reactor is 20 × 5 × 6 mm^3. A horseshoe magnet on the top is used to align particles. The center of the well has a small hole at the bottom sealed by a glass coverslip for microscopy. Two types of particles coated by either streptavidin or anti-DIG (blue and red) are aligned by the magnetic field into a string of a random sequence. λ-DNA linkers (black) have heterogeneous chain ends. Conjugation between the antibody coated on the particles and biotin or DIG tagged to the chain ends is highly selective. Neighboring particles are bridged by the λ-DNA linkers only when they are different types. (b) (Top left) Mixture of fluorescently labeled λ-DNA linkers and mPEG-NH_2-coated PS (d = 5.7 μm) spheres after an overnight reaction. Particles are well-dispersed and DNA linkers are not bound to the particles. (Bottom left) PS spheres (d = 4.7 μm) coated with mPEG-NH_2 and anti-DIG, mixed with the same DNA linkers after an overnight reaction. The DIG-capped end of DNA is bound to the reactive anti-DIG sites of the spheres while the other biotin-capped end remains unbound. (Right) Image of the synthesized DNA-bridged dumbbells highlighted by yellow rectangles after removing the magnetic field. Half of the particles (d = 2.9 μm) are anti-DIG-coated and the other half are streptavidin-coated. Scale bars = 5 μm.

react with two different batches of particles. One batch of particles was treated with mPEG-NH_2 only for passivation, while the particles in the other batch had conjugated reactive sites (anti-DIG) on their surfaces in addition to mPEG-NH_2. First, mPEG-NH_2 made the particles well-dispersed and free of aggregation in both cases. Thus, dumbbells form because of the bridging of DNA linkers, instead of any nonspecific interparticle interactions. When there was no anti-DIG conjugated to the particle surface, the fluorescently labeled λ-DNA molecules exhibited free diffusion without being adsorbed to the particles (Figure 1b top left). In contrast, for anti-DIG-coated particles, the DIG-capped end of the fluorescent λ-DNA was bound to the particle surface while the biotin-capped end remained unbound (Figure 1b bottom left). This control experiment proved that our synthetic method can successfully suppress nonspecific DNA−particle binding and particle−particle aggregation. Figure 1b (right) shows a representative product of the synthesis after the magnetic field was removed. As expected, most of the particles were singlets or dimers. The dumbbells were tightly bound in the absence of external flows due to the self-depletion of long DNA linkers. As our λ-DNA was long compared to the size of the particles, the bridging DNAs were entropically excluded from the interparticle gaps, which induced attractive forces between linked particles.[45−48] When the dumbbells were subjected to shear-banding flows, particles in the dumbbells showed separations longer than the particle diameter, illustrating the stretching of bridging DNAs. The depletion interaction was significantly reduced when the dumbbells were submerged in high-concentration entangled DNA solutions, where the particles were surrounded by not only DNA linkers but also high-concentration background DNA chains in solution.

2.2. Sample Preparation and Characterization. Calf-thymus DNA (Sigma-Aldrich, 10−15 kbp) was dissolved in dumbbell suspensions as a background polymer at a fixed concentration of 11.3 mg/mL, which is 87 times its overlap concentration. The mixture was left for at least a week with occasional gentle stirring to ensure its equilibration. We estimated the average radius of gyration R_g of the background DNA to be 0.25 μm based on the R_g of λ-DNA.[35] We performed shear rheology measurement (DHR, TA Instruments) in both linear and nonlinear viscoelastic regions to characterize the material properties of the solution. Rheological characterizations were performed with the 40 mm parallel plate geometry at 21.0 °C (Advanced Peltier Plate, TA Instruments) in order to ensure sufficient torque signal and good temperature control. To mitigate the effect of concentration drift due to solvent evaporation, a solvent trap was used to provide saturated water vapor and prevent solvent evaporation for the duration of the rheological measurements.

We first performed small amplitude oscillatory shear (SAOS) experiments to characterize the linear viscoelastic response of the solution. From the dynamic amplitude sweep data at 1 rad/s, the system remains in the linear viscoelastic region up to oscillatory strain amplitude of 10% (Supporting Information). Based on the dynamic oscillatory shear test result (Figure 2a), our DNA solution behaves similar to a critical gel: in the low-frequency region, both the storage (G') and the loss moduli (G'') become congruent and scale with $\omega^{1/2}$, which satisfies the Winter−Chambon criterion for the gel point.[49,50] This apparent gel-like behavior cannot be due to the presence of chemical cross-links absent from our system, but rather from the physical cross-links of the highly concentrated DNA network,[51] which may arise from hydrogen bonding or ionic coordination due to residual ionic interactions in the solution.[52,53] The plateau modulus (G_N^0) should be larger than 10^2 Pa, even though we cannot access its exact value from the SAOS measurements due to the inertia of the rheometer at high oscillatory frequencies.

The result of the SAOS experiment shows the gel-like behavior of the concentrated DNA solution at low shear rates and shear amplitudes. To probe the flow behavior of the solution under strong shear relevant to our large amplitude oscillatory shear (LAOS) experiments below, we also performed a series of controlled step strain rate tests to characterize the nonlinear rheological properties of the sample. We imposed a step strain rate ranging from 0.01 up to 100 s^{-1}, and the steady shear viscosity was measured at each shear rate. Even at the lowest shear rate of 0.01 s^{-1}, where the stress signal is barely above the noise floor of our rheometer, we observed no apparent yield stress and the sample was deformed and flowed like a liquid (Supporting Information). The observation suggested that the gel structure observed in SAOS is extremely weak. When the shear rate is greater than or equal to 0.05 s^{-1}, we reached the steady-state response of the system, which was consistent with that of a shear-thinning fluid (Figure 2b). Moreover, our DNA solution obeys the Cox−Merz rule (Figure 2b), which is known to be applicable for polymeric fluids without chemical cross-links but is invalid for weak gels.[54,55] Taken together, these rheological behaviors showed that the gel-like structure formed in the quiescent state was so weak that it could be fully disrupted by subjecting the sample to a steady shear flow with a shear rate as low as 0.05 s^{-1}. Thus, under LAOS used in our study here with shear rates around 60 s^{-1} and shear strain around

https://doi.org/10.1021/acs.macromol.0c02890
Macromolecules 2021, 54, 4186−4197

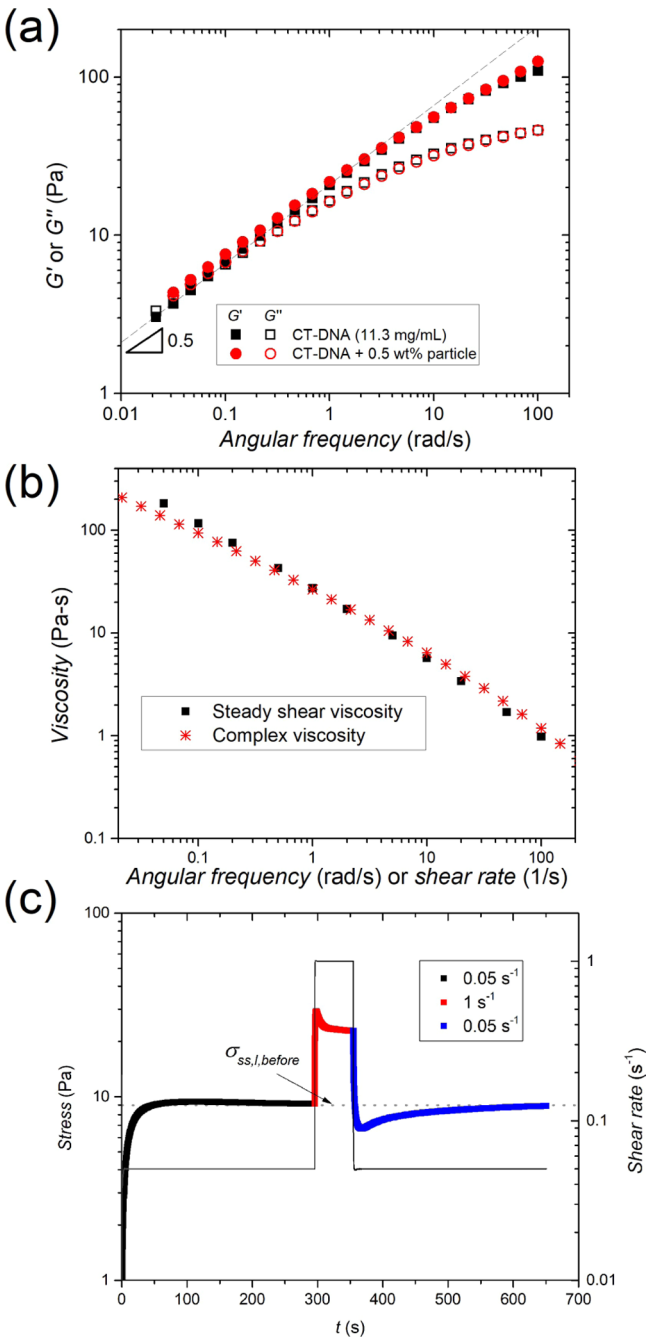

Figure 2. Rheological characterization of concentrated calf-thymus DNA (CT-DNA, M_w = 10−15 kbp) solution in TBE 1× buffer at a concentration of 11.3 mg/mL. All measurements were performed at 21 °C. (a) Linear viscoelasticity of the concentrated CT-DNA solution with and without magnetic tracer particles. Both storage (G') and loss (G'') moduli at the low-frequency region (<0.1 rad/s) become congruent and scale with $\omega^{1/2}$ (dashed line), suggesting that the system is at the gel point. Neither G' nor G'' moduli was affected by the addition of magnetic tracer particles (0.5 wt %). (b) Steady-state shear viscosity and complex viscosity of the CT-DNA solution, which follows the Cox-Merz rule. (c) Shear stress from a rate-switching experiment, performed by stepping up and down the shear rate between $\dot{\gamma}_l$ = 0.05 s^{-1} and $\dot{\gamma}_h$ = 1.0 s^{-1}. The steady shear stress at $\dot{\gamma}_l$ (the dashed line) was independent of the shear history, and the relaxation time for the disrupted sample to recover its steady state was τ = 77 s.

250%, the weak attraction between DNA molecules that gives rise to the weak gel behavior observed in the SAOS measurements becomes negligible and does not affect the flow behaviors of our concentrated DNA solutions.

To illustrate this point further, we also conducted a series of rate-switching shear experiments.[56] We first applied a low "probing" shear rate ($\dot{\gamma}_l$) until the shear stress reached a steady state. Then, the shear rate was stepped up to a high "disrupting" shear rate ($\dot{\gamma}_h$), which is sufficiently high to fully disrupt any initial gel-like structure in the quiescent system. After the sample had reached the steady state at $\dot{\gamma}_h$, we stepped down the shear rate back to $\dot{\gamma}_l$ to reach the steady state at $\dot{\gamma}_l$ again. If there were any partially broken gel structures remaining in the sample at the initial steady state at $\dot{\gamma}_l$, the steady shear stresses at $\dot{\gamma}_l$ measured before and after the disrupting shear would display a noticeable difference. In the main text, we examined the case where $\dot{\gamma}_l$ = 0.05 s^{-1} and $\dot{\gamma}_h$ = 1.0 s^{-1} (Figure 2c). Results from other several pairs of $\dot{\gamma}_l$ and $\dot{\gamma}_h$ are available in the Supporting Information. Figure 2c shows that the steady shear stress measured at $\dot{\gamma}_l$ = 0.05 s^{-1} is independent of the shear history of the sample. The difference between the steady-state shear stresses before and after $\dot{\gamma}_h$ is only 3.4%, smaller than the resolution of the rheometer. The finding again suggested that the gel-like structure has been completely disrupted at $\dot{\gamma}_l$ = 0.05 s^{-1} and the gel structure observed in SAOS was indeed very weak. The results from both step-strain and rate-switching experiments ensured that our measurements of the shear banding of the DNA solution in the following using LAOS should be hardly affected by the effect of the initial gel-like structure formed in the quiescent state. Since the gel structure is fully disrupted under strong shear of LAOS, any spatially heterogeneous dynamics shown in our study cannot be due to the remnant gel structures in the solution.

The transient stress response following the step-down of the shear rate arises due to the reversible formation of physical polymer chain networks in the concentrated solution.[56] Thus, from the series of rate-switching shear experiments (Figure 2c), a relaxation time (τ) can be estimated, which gives the characteristic time scale required for the sample solution disrupted by $\dot{\gamma}_h$ to recover its steady-state structure at $\dot{\gamma}_l$.[56] Specifically, we fit the stress relaxation data after the stepping down of the shear rate with an empirical, single-mode stress relaxation model

$$\frac{\sigma_\infty^* - \sigma(t)}{\sigma_\infty^* - \sigma_{min}} = e^{-t/\tau} \quad (1)$$

where σ_{min} is the stress at the minimum of the undershoot, t is the elapsed time after σ_{min} is reached, and σ_∞^* and τ are fitting parameters corresponding to the steady-state shear stress after disruption and the relaxation time, respectively. We estimated τ = 77 s based on the data at $\dot{\gamma}_h$ = 1.0 s^{-1} and $\dot{\gamma}_l$ = 0.05 s^{-1}. Since 0.05 s^{-1} is high enough to disrupt the weak gel structure in the solution, the relaxation process at $\dot{\gamma}_l$ = 0.05 s^{-1} following $\dot{\gamma}_h$ should be dominated by the reconstruction of the steady-state conformation of the DNA chains, rather than the reformation of the weak gel-like structure. Note that τ is a function of both $\dot{\gamma}_h$ and $\dot{\gamma}_l$.[56] Increasing $\dot{\gamma}_h$ at a fixed $\dot{\gamma}_l$ or decreasing $\dot{\gamma}_l$ at a fixed $\dot{\gamma}_h$ would lead to an increase in τ. Hence, to obtain the best estimate of the longest relaxation time, we chose the highest possible $\dot{\gamma}_h$ without potential edge effects from the rheometer and the lowest possible $\dot{\gamma}_l$ that is sufficient to disrupt the quiescent gel structure. Thus, τ = 77 s gives the best estimate of the lower bound of the longest relaxation time of our DNA solution. A more detailed discussion of τ at different $\dot{\gamma}_l$ and $\dot{\gamma}_h$ is provided in the Supporting Information.

One should note that even though our concentrated DNA solution is highly shear-thinning (Figure 2b), its steady shear viscosity does not exhibit $\eta \sim \dot{\gamma}^{-1}$, which would otherwise lead to the well-known criterion of the steady shear banding, $\sigma = \eta\dot{\gamma} \sim \dot{\gamma}^0$.[57] Instead, the constitutive curve of the sample solution grows monotonically with increasing shear rates. This behavior suggests that the shear banding observed in our LAOS experiments below should be a time-dependent shear banding accompanied by a strong overshoot of the transient shear stress/viscosity, rather than the steady shear banding

https://doi.org/10.1021/acs.macromol.0c02890
Macromolecules 2021, 54, 4186−4197

signified by the steady shear stress plateau over a range of strain rates resulting from the constitutive instabilities.[58]

It is also worth noting that the material parameters, such as τ and G_N^0, extracted from the rheological test, provide only crude estimates. The weak gel behavior of our samples at low shear frequencies prevents us from reaching the terminal relaxation via SAOS. Instead, we estimated τ from the transient shear experiments, where strong nonlinear shear breaks the weak intermolecular interactions and re-establishes the fluid behavior of the samples at high shear rates and strains. Moreover, unlike λ-DNA, the calf-thymus DNA is much more polydisperse. There are an appreciable fraction of DNA chains longer than the average molecular weight of the sample, which may introduce additional complexity to the interpretation of the terminal relaxation time. Nevertheless, a recent simulation demonstrated that polydispersity suppresses the onset of time-dependent shear banding.[59] Thus, polydispersity cannot be the leading factor triggering the shear banding observed in our experiments shown below. While the gel-like behavior at low shear frequencies and the polydispersity of the calf-thymus DNA molecules certainly complicate the interpretation of τ and G_N^0 from the rheological measurements, the conclusion drawn from our experimental results reported below is independent of the exact numerical values of these parameters.

Finally, the addition of 0.5 wt % magnetic tracer particles affected neither the linear (Figure 2a) nor nonlinear (Supporting Information) rheological characteristics of the DNA solution due to the low particle volume fraction in the system. Therefore, we assume that the rheological parameters determined from the DNA solutions without magnetic particles can be used to describe the solutions that contain a small fraction of the DNA-bridged dumbbells of similar concentrations.

2.3. Experimental Setup and Procedure. The sample solution was injected into our custom-built planar-Couette confocal shear cell (Figure 3a), which consisted of two square-cut glass coverslips (5 × 5 mm^2) aligned in parallel. While the top plate was fixed, the bottom plate was driven sinusoidally using a piezoelectric actuator to exert LAOS with strain $\gamma(t) = \gamma_0 \sin(2\pi ft) = (A_0/H)\sin(2\pi ft)$, where A_0 is the amplitude of applied shear displacement, H is the separation between the plates, and f is the shearing frequency. The amplitude of the velocity of the bottom plate is $V_0 = 2\pi fA_0$. Detailed information about our shear cell can be found in refs 60−62. In our experiments, we fixed A_0 = 150 μm, H = 60 μm (= 240R_g), and f = 4.0 Hz, which give the apparent Weissenberg number $Wi = \tau V_0/H$ = 770 and the Deborah number De = $2\pi f\tau$ = 1940. Note that our shear protocol is within the range of the shear rates and strains where the strong stress overshoot emerged (Figure S1c). We defined a coordinate system so that x is along the flow direction, y is along the shear gradient direction, and z is along the vorticity direction of the shear.

The shear cell was placed on an inverted confocal microscope for visualization of the fluid flow via the transparent bottom plate. We used a 20× dry objective (NA = 0.50) to access a large field of view. The depth of field was about 2.0 μm. Our previous study showed an abnormally long penetration depth of edge disturbance in the shear-banding polymer flows.[63] Thus, to avoid the edge effect, we performed measurements at least 20H away from all the edges. At the fixed x and z position, we varied y to construct a velocity profile using particle image velocimetry. Typically, image sequences were taken at 11 different heights and the whole y range was scanned three times for error estimation. It took about 1 min to acquire all 33 videos required for a single shear profile. In addition to velocity profiles, we also analyzed the dynamics of immersed dumbbells via particle tracking velocimetry (PTV). In particular, we took strobed image sequences by synchronizing the imaging frequency with the shearing frequency, that is, at a frame rate of 4.0 Hz. The resulting images are snapshots of the particle positions at a fixed phase of the LAOS cycle. To reduce possible distortion of images due to the finite exposure time, each snapshot in an image sequence was taken once in a shear cycle when the applied shear strain is at its maximum and the corresponding shear rate reaches its minimum.

For each image sequence, we first tracked the trajectories of all the identified particles using a standard PTV algorithm.[64] The net drift of particles quantified by $\langle \Delta x \rangle$ and $\langle \Delta z \rangle$ was subtracted, where the average was taken over all the particles in the sequence. We then ran a custom MATLAB code to select dumbbells from all the tracked particles (Supporting Information). With the strict dumbbell selection rule, we made sure that all the colloidal pairs identified were true DNA-bridged dumbbells.

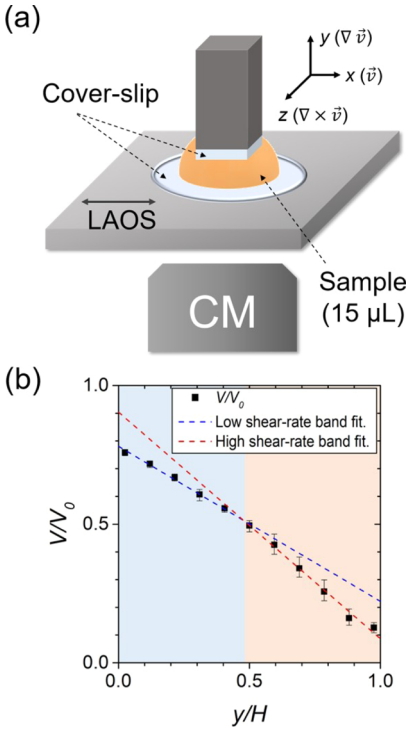

Figure 3. Experimental setup and shear-banding velocity profile. (a) Schematic of the custom-built planar-Couette shear cell (not to scale). CM: a confocal microscope. (b) Velocity profile of the concentrated DNA solution at apparent Wi = 770 and De = 1940. The profile is fitted piece-wise with two linear regressions. The low-SRB with the smaller shear gradient is colored in blue, whereas the high-SRB with the larger shear gradient is colored in red. The same color code is applied throughout the paper.

3. RESULTS

3.1. Shear-Banding Flows. A typical shear profile is shown in Figure 3b. The velocities and heights are normalized by the velocity amplitude (V_0) and the gap thickness (H), respectively. The profile can be well-fitted by piece-wise double-linear functions. The low-shear-rate band (SRB) appears near the bottom moving boundary and the high-SRB forms near the top stationary boundary. Mild wall slips are observed near both the top and bottom plates. Wi = 705 in the high-SRB and Wi = 594 in the low-SRB. In the current study, we focused on the dynamics of embedded dumbbells in two coexisting shear bands in a shear-banding flow. Thus, we chose a representative experimental condition, where an unambiguous shear banding can be observed. Our previous work on entangled DNA solutions has explored the shear-banding dynamics and the degree of wall slips in a much larger phase space and showed shear-banding velocity profiles over a wide range of Wi by varying the shear frequency and the gap thickness of the shear cell.[65] A phase diagram has been provided in ref 65.

Strobed image sequences are taken at y/H = 0.05, 0.15, 0.25, 0.35, 0.55, 0.65, 0.75, and 0.85. The first four heights are inside

https://doi.org/10.1021/acs.macromol.0c02890
Macromolecules 2021, 54, 4186−4197

the low-SRB, whereas the last four heights are inside the high-SRB. Applying the strict dumbbell selection rule (see the Supporting Information) to the strobed image sequences produces more than 800 trajectories of dumbbells in each shear band. We then extract the center of mass, the orientation, and the projected interparticle distance of these dumbbells over time. Since the imaging plane of our confocal microscope is in the $x-z$ plane with a depth of view in the y direction of about 2 μm, the center of mass and the interparticle distance represent the 2D projection of the 3D configuration of dumbbells (Figure 1b right). The center of mass of a dumbbell is determined from the midpoint of the $x-z$ projection of the vector connecting the centers of the two linked particles, whereas the length of the projected vector gives the projected interparticle distance l (Figure 4). The orientation of a dumbbell is quantified by its azimuthal angle with respect to the flow (x) direction, θ. For ease of visualization and comparison of features in the two coexisting shear bands, the data acquired from the low-SRB will be blue-colored, while the data for the high-SRB will be red-colored in the following sections.

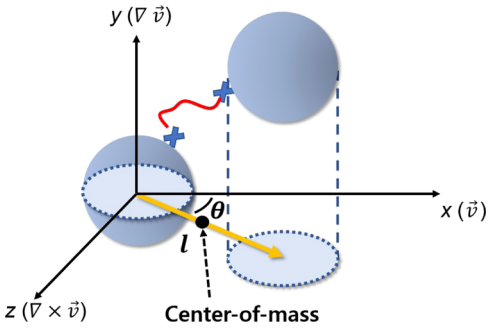

Figure 4. Schematic of a dumbbell linked by a DNA linker (red) projected onto the imaging plane (the $x-z$ plane). The yellow vector connects the 2D-projected centers of mass of the two linked particles. The center of mass of the dumbbell is determined by the midpoint of the vector. The magnitude of the vector gives the projected interparticle distance l. The orientation of the dumbbell is characterized by the azimuthal angle, θ, with respect to the flow (x) direction.

3.2. Orientation of Dumbbells in Shear-Banding Solutions. We first study the relative orientation of dumbbells in the two shear bands. Taking one of the two linked particles as the origin, the projected position of the other particle in a dumbbell is displayed as a 2D probability distribution function (PDF) in Figure 5. In the low-SRB, we find that PDF exhibits bimodal peaks, one along the flow (x) direction and the other along the vorticity (z) direction (Figure 5a). In contrast, in the high-SRB, the distribution becomes unimodal with most of the dumbbells aligning along the flow (x) direction (Figure 5b).

The alignment of an anisotropic slender body along the vorticity direction in a sheared viscoelastic fluid—the so-called log-rolling configuration—has been experimentally reported.[66−68] The log-rolling alignment was attributed to normal stress differences that drive the slender bodies to drift toward the vorticity direction through Jeffery orbits.[69] At higher shear rates or, equivalently, at higher elasticities, the reorientation of the log-rolling slender body toward the flow direction has also been predicted and observed experimentally,[66,67,70] which lead to bimodal distributions similar to that shown in Figure 5a. Thus, while normal stress differences drive

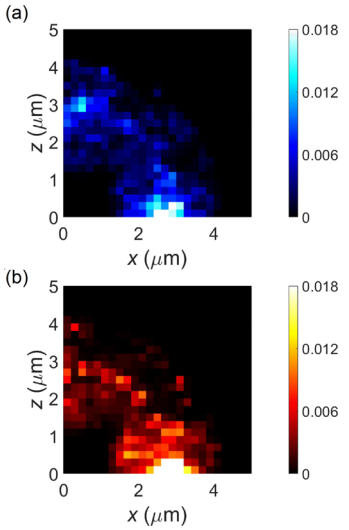

Figure 5. Dumbbell orientation in shear-banding solutions. (a) PDF of the projected orientation of dumbbells in the low-SRB. The bimodal peaks along the flow (x) direction and along the vorticity (z) direction are pronounced. (b) PDF of the projected orientation of dumbbells in the high-SRB. The single peak along the flow (x) direction is noticeable.

dumbbells toward the vorticity direction, elasticity preferably aligns them along the flow direction. In the low-SRB of our concentrated DNA solutions, normal stress differences and elastic stresses are presumably comparable, resulting in the bimodal distribution (Figure 5a). In the high-SRB, the high shear rate and strong elasticity reduce the degree of log rolling and force the dumbbells to be more flow-aligned (Figure 5b). Different dumbbell orientational distributions reflect the shift of the relative contributions of normal and elastic stresses in the two coexisting shear bands. Thus, imaging the local conformation of dumbbells allows us to resolve qualitatively the spatial variation of different stress components in concentrated polymer solutions, which cannot be achieved by either macroscopic rheology or shear profile measurements.

3.3. Dynamics of Dumbbells in Shear-Banding Solutions. We also analyze the translational and rotational dynamics of DNA-bridged dumbbells in the two coexisting shear bands. Our previous experiments have studied the translation of spherical tracers in shear-banding DNA solutions.[65] In the high-SRB, the mean-squared displacements (MSDs) of spherical tracers in the x and z directions, defined as $\langle \Delta x(t)^2 \rangle = \langle [x(t_0 + t) - x(t_0)]^2 \rangle$ and $\langle \Delta z(t)^2 \rangle = \langle [z(t_0 + t) - z(t_0)]^2 \rangle$, respectively, are subdiffusive at short times, display superdiffusive motions at intermediate times with $\langle \Delta x(t)^2 \rangle$ and $\langle \Delta z(t)^2 \rangle \sim t^{1.4}$, and eventually become diffusive with $\langle \Delta x(t)^2 \rangle$ and $\langle \Delta z(t)^2 \rangle \sim t$ in the long time limit. On the contrary, the MSDs of spherical tracers in the low-SRB transition from subdiffusive to diffusive dynamics without exhibiting the intermediate superdiffusive regime. Furthermore, the MSDs in the x direction are significantly greater than the MSDs in the z direction, indicating anisotropic tracer dynamics in shear-banding flows. The degree of anisotropy quantified by $\langle \Delta x(t)^2 \rangle / \langle \Delta z(t)^2 \rangle$ appears greater in the high-SRB than in the low-SRB. Note that the translational MSDs in the shear frame obtained from the strobed image sequence in our experiments are equivalent to the MSDs of nonaffine motions analyzed in previous studies on supercooled colloidal liquids under shear.[71]

https://doi.org/10.1021/acs.macromol.0c02890
Macromolecules 2021, 54, 4186−4197

The translational dynamics of dumbbells are also anisotropic with $\langle \Delta x(t)^2 \rangle > \langle \Delta z(t)^2 \rangle$ in both shear bands (Figure 6a). The

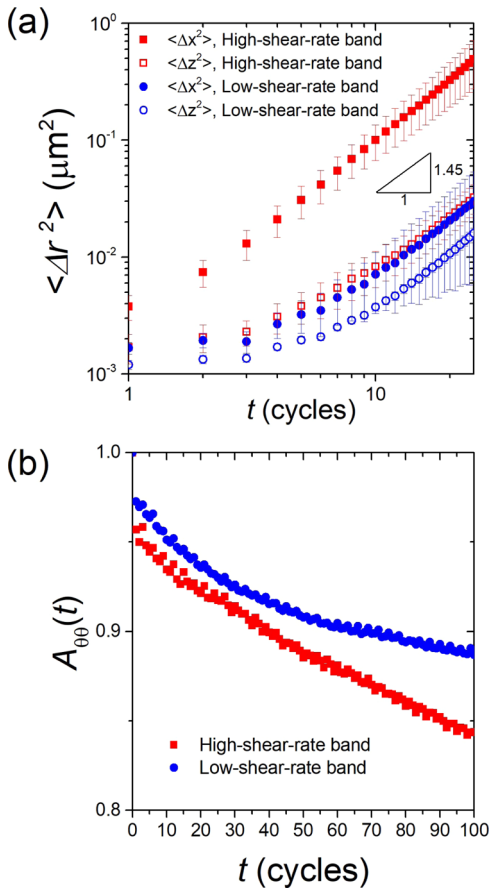

Figure 6. (a) Translational MSDs of dumbbells in the two coexisting shear bands. Superdiffusive scaling with a slope of 1.45 is indicated for reference. (b) Autocorrelation of dumbbell orientation, $A_{\theta\theta}(t)$, in the two coexisting shear bands.

degree of anisotropy is stronger in the high-SRB, similar to the behaviors of spherical tracers. In the high-SRB, the motions are subdiffusive at short times and become superdiffusive at intermediate times with $\langle \Delta x(t)^2 \rangle$ and $\langle \Delta z(t)^2 \rangle \sim t^{1.45}$ (Figure 6a). We expect the translational motions to be diffusive in the long time limit, which is beyond the time scale of our current experiments. While the dumbbells in the high-SRB behave similarly to the spherical tracers in the high-SRB of our previous study,[65] the MSDs of the center of mass of the dumbbells in the low-SRB do not follow the reported behavior of spherical tracers in the low-SRB. The MSDs of the dumbbells in the low-SRB display superdiffusive motion after the initial subdiffusive motion (Figure 6a), instead of transitioning directly to diffusive motion. To determine whether the dissimilar trend of the dumbbells in the low-SRB is due to the difference between dumbbells and spherical tracers, we also analyze the MSD of the coexisting spherical tracers in the low-SRB. The MSD of the spherical tracers in the present study shows the same trend as the coexisting dumbbells, which indicates that the behavior is not specific to the dumbbells. It implies that the transition from subdiffusive to diffusive dynamics in the low-SRB of our previous study may depend on specific experimental conditions.[65] In particular, the calf-thymus DNA in the present study (10−15 kbp) is shorter than the DNA used previously (75 kbp)[65] and thus less-entangled. To achieve shear-banding flows, the applied strain ($\gamma_0 = 2.5$) in the current study is two times higher than the strain in the previous study ($\gamma_0 = 1.2$). Despite the difference, we find that the MSDs of the translation of dumbbells in the high-SRB are drastically enhanced compared with the MSDs in the low-SRB in both studies. The fast dynamics of dumbbells in the high-SRB indicate the low effective viscosity of the entangled polymer solution in that band.

The anisotropic shape of the dumbbells allows us to further investigate their rotational dynamics, which cannot be achieved using spherical tracers. The azimuthal orientation of dumbbells, θ, is defined in Figure 4. We quantify the relaxation of the rotational fluctuations of dumbbells around their shear-induced stable orientations via the autocorrelation of θ, $A_{\theta\theta}(t) \equiv \langle [\theta(t_0 + t) - \overline{\theta}][\theta(t_0) - \overline{\theta}] \rangle / \langle [\theta(t_0) - \overline{\theta}]^2 \rangle$, where $\theta(t)$ is the dumbbell orientation at time t and $\langle \cdots \rangle$ averages different dumbbells at different t_0. $\overline{\theta}$ is the long-time average of the orientation of the specific dumbbell under consideration at t_0, which gives the stable orientation of the dumbbell under shear. Because the orientation of dumbbells in the high-SRB displays a single peak along the flow direction (Figure 5b), $\overline{\theta} = 0$. In the low-SRB, on the other hand, the distribution of dumbbell orientation exhibits bimodal peaks, one along the flow direction and the other along the vorticity direction (Figure 5a). Thus, $\overline{\theta}$ equals to either 0 or $\pi/2$. Assuming rotational fluctuations of dumbbells are sufficiently small, a dumbbell with $\theta(t_0)$ close to 0 will have $\overline{\theta} = 0$. A dumbbell with $\theta(t_0)$ close to $\pi/2$ will relax to $\overline{\theta} = \pi/2$ at long times. Figure 6b shows $A_{\theta\theta}(t)$ in the low- and high-SRBs, which shows a clear difference in the two coexisting bands. The dumbbells in the high-SRB relax significantly faster than those in the low-SRB. Similar to the translational degree of freedom, the rotational motion in the low-SRB is greatly retarded compared with that in the high-SRB. Thus, both the translation and rotation of dumbbells show enhanced dynamics and suggest low effective viscosity in the high-SRB.

To further explore the translation and rotation of dumbbells, Figure 7 plots the PDF of angular and translational displacements during a time interval of 10 cycles. Here, we characterize the total translational displacement using $\Delta r = (\Delta x^2 + \Delta z^2)^{1/2}$. Since translational dynamics are dominated by the motion in the x direction, qualitatively similar results can be also obtained when $\Delta r = |\Delta x|$ alone is used. The translational and angular displacements of the dumbbells in the high-SRB decay more slowly than those in the low-SRB and exhibit long non-Gaussian tails. The effect is more pronounced for translation. Dumbbells in the high-SRB experience rapid translation and rotation more frequently than those in the low-SRB. More importantly, based on our previous study on the dynamics of spherical tracers,[65] the long tails in the PDFs suggest spatial heterogeneity of tracer dynamics in the high-SRB. The suggestion is indeed consistent with our direct observation. While most of the dumbbells show slow translation and rotation in the high-SRB, a few dumbbells in that band exhibit fast translation and rapid rotation during the same time interval (Video S1), which give rise to the enhanced translational and rotational dynamics and the long PDF tails in the high-SRB. Interestingly, particles experiencing fast translation tend to show rapid rotation too. The observation inspires us to examine the coupling between translation and rotation of dumbbells next.

https://doi.org/10.1021/acs.macromol.0c02890
Macromolecules 2021, 54, 4186−4197

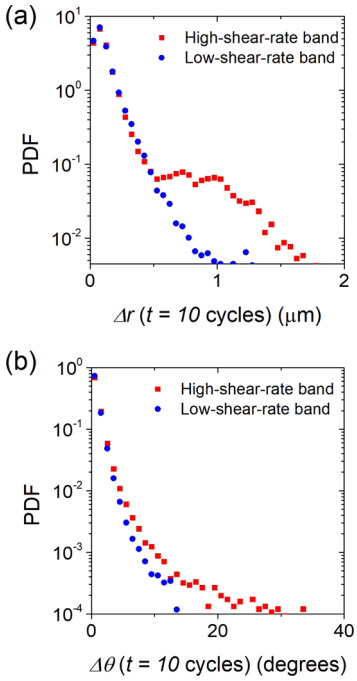

Figure 7. PDFs of translational and rotational displacements of dumbbells during a time interval of 10 cycles in the two coexisting shear bands. (a) PDFs of the translational displacement over 10 cycles in low-(blue) and high-(red) SRB. (b) PDFs of the rotational displacement over 10 cycles in low-(blue) and high-(red) SRB.

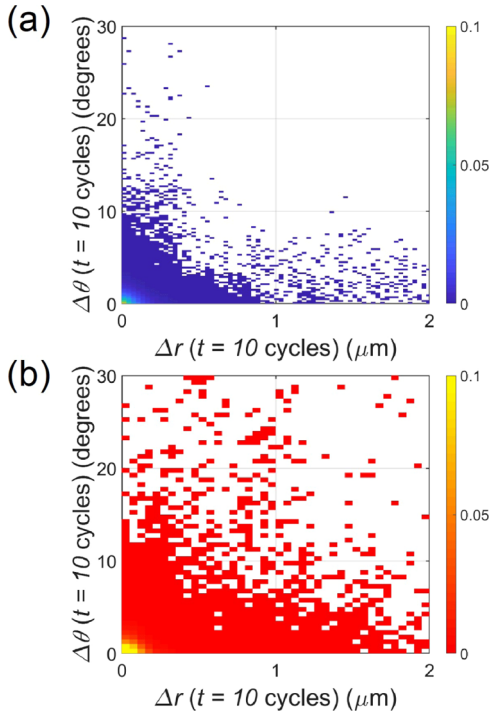

Figure 8. Correlation of translation and rotation of dumbbells in shear-banding DNA solutions. 2D PDF of the translational and angular displacements of dumbbells over a time interval of 10 cycles in the low-SRB (a) and in the high-SRB (b). Points in the upper right region of the plot indicate the positive correlation between fast translation and rapid rotation.

We find that the enhanced translational and rotational dynamics of dumbbells in the high-SRB are coupled. Figure 8a,b shows the 2D PDFs of translational and rotational displacements of dumbbells over a time interval of 10 cycles. In the low-SRB, translation and rotation of dumbbells are independent; very few fast translating dumbbells rotate rapidly and vice versa. In comparison, in the high-SRB, the probability that a dumbbell experiences both fast translation and rapid rotation is much higher. The observation that fast translating dumbbells likely rotate faster in the high-SRB suggests the change in the local structure of concentrated DNA solutions under strong shear in the high-SRB, which promotes the local translational and rotational dynamics of embedded dumbbells simultaneously.

3.4. Interparticle Separation of Dumbbells in Shear-Banding Solutions. Finally, as dumbbells are bridged by long linear DNA molecules, the interparticle distance projected onto the $x-z$ plane allows us to extract the information on chain extension in sheared concentrated DNA solutions. Figure 9a plots the PDF of the projected interparticle separation of λ-DNA-linked dumbbells, l, in the high-SRB. As a comparison, we also show the PDF of nonextensible dumbbells linked by short DNA linkers of 12 base pairs. For nonextensible dumbbells, the probability of $l > d$ approaches zero as expected, where $d = 2.9$ μm is the diameter of linked colloidal particles. A small nonzero probability at $l/d > 1$ is due to the uncertainty in particle tracking. In contrast, λ-DNA-linked dumbbells exhibit strong sheared-induced extension with $l > d$. A small peak in the PDF is observed above $l/d = 1.2$.

How does the shear-induced extension of the DNA linkers of a dumbbell correlate with the dynamics of the dumbbell? To answer the question, we compute the cross-correlation between the projected interparticle separation of a dumbbell at an initial time t_0, $l(t_0)$, and its subsequent translational displacement $\Delta r(t)$ over a time interval t from t_0 to $t_0 + t$,

$$C_{l,\Delta r}(t) = \frac{\langle [l(t_0) - \langle l(t_0)\rangle_N][\Delta r(t) - \langle \Delta r(t)\rangle]\rangle_{t_0,N}}{\sigma_l \sigma_{\Delta r}} \quad (2)$$

where σ_l and $\sigma_{\Delta r}$ are the standard deviations of l and Δr. The operator $\langle \cdots \rangle_N$ takes the average of all the dumbbells in each band, whereas $\langle \cdots \rangle_{t0,N}$ takes the average of all the dumbbells in the same band and all the initial times. $C_{l,\Delta r}(t)$ thus aims to quantify how the stretching of a dumbbell correlates with its translation at later times. However, it should be noted that the interparticle separation we measure directly in experiments is the 2D projection of the true interparticle distance (see Figure 4). Hence, $C_{l,\Delta r}$ also measures the potential correlation between the orientation and the translation of dumbbells in shear flows. Indeed, a negative correlation between l and Δr is expected even for nonextensible dumbbells in Newtonian solvents under LAOS with uniform shear (Supporting Information). Such a negative correlation arises from the coupling between the anisotropic diffusivity of dumbbells and the background shear flow in analogy of Taylor dispersion.[72−74] To eliminate this diffusion−convection coupling of dumbbells of different orientations, we focus on the behaviors of dumbbells preferentially oriented within the $x-z$ plane in our analysis. Such dumbbells can be successfully selected by requiring l to be longer than a cutoff length $l_{cut} > d$. Based on the PDF of l (Figure 9a), we choose $l_{cut} = 1.2d$ in our analysis so that any dumbbells with $l \geq l_{cut}$ are guaranteed to be stretched and preferentially align in the $x-z$ plane. Varying l_{cut} within the limit of $l_{cut} > d$ does not qualitatively change the result.

https://doi.org/10.1021/acs.macromol.0c02890
Macromolecules 2021, 54, 4186−4197

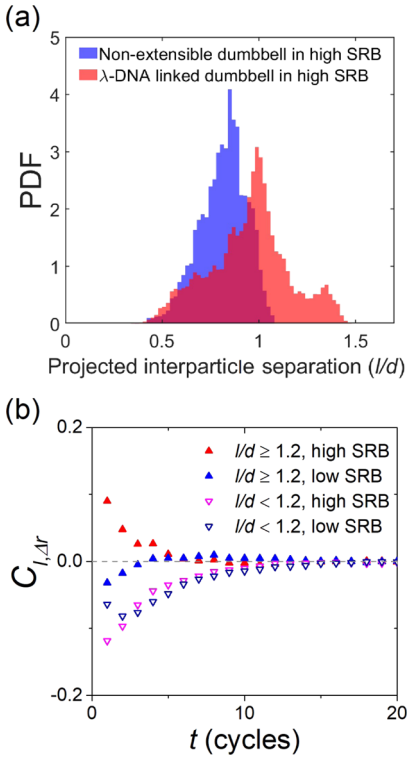

Figure 9. Correlation between dumbbell dynamics and chain extension. (a) PDF of the projected interparticle separation l in the high-SRB. l is normalized by the diameter of linked colloidal particles d = 2.9 μm. While l is upper-bounded by the particle diameter for nonextensible dumbbells (blue), the dumbbells bridged by long λ-DNA linkers can have $l > d$, indicating the stretching of the linkers. (b) Correlations between the in-plane translational displacement and the chain extension for dumbbells in four different classes according to whether $l/d \geq 1.2$ and whether they are in the low- or high-SRB. The data with $l/d \geq 1.2$ are described with filled symbols, whereas $l/d < 1.2$ data are drawn with hollow symbols. Upper triangles indicate data in the high-SRB, while lower triangles indicate data in the low-SRB.

Figure 9b shows $C_{l,\Delta r}(t)$ for dumbbells with $l \geq l_{cut}$ in both high- and low-SRBs. As a comparison, we also show the correlations of dumbbells with $l < l_{cut}$. First, all the correlations approach zero over a long time interval as expected. In the long time limit, a dumbbell samples all the possible orientations in the shear flow and therefore experiences all different degrees of chain extension. Any possible correlation between the initial chain orientation/extension and the subsequent translation of the chain is lost in the long-time limit. At short times, however, dumbbells with $l \geq l_{cut}$ in the low-SRB, as well as all the dumbbells with $l < l_{cut}$ regardless of their location, all exhibit negative correlations between l and Δr, similar to that of nonextensible dumbbells in pure solvents (Supporting Information). The result suggests that these correlations are dominated by the diffusion-convection coupling. More importantly, dumbbells with $l \geq l_{cut}$ display a positive correlation between l and $\Delta r(t)$ in the high-SRB at short times. Such a finding provides direct evidence on the relation between local chain extension and low-viscosity zones in the high-SRB. Similarly, the cross-correlation of the interparticle separation l and $\Delta\theta$ also shows a noticeably positive correlation for the dumbbells with $l \geq l_{cut}$ in the high-SRB (Figure S4). It again suggests that the local low-viscosity zones with fast dumbbell dynamics are coupled with the regions of chain extension. The implication of our observations on the physical mechanism of shear banding shall be discussed next.

4. DISCUSSION

Taken together, our results show that the conformation and dynamics of DNA-bridged dumbbells exhibit qualitatively different features in the low- and high-SRBs in concentrated DNA solutions. In the high-SRB, dumbbells show a preferential alignment along the flow direction, implying strong local shear with dominant elastic stress components. More importantly, both translational and rotational dynamics of dumbbells become spatially heterogeneous in the high-SRB. A fraction of dumbbells in the band exhibit strongly correlated fast translation and rapid rotation with pronounced chain extension.

Based on our experimental observations, we revisit the existing mechanisms proposed for shear banding in concentrated polymer fluids. Phenomenological one-fluid models provide universal criteria for the onset of both steady and time-dependent shear banding.[23,39] Shear banding in steady shear flows arises from the mechanical instability associated with nonmonotonic constitutive relations, whereas time-dependent shear banding is usually accompanied by strong stress overshoots. Since our DNA solution displays a monotonic relationship between shear stress and shear rate based on a separate cone-plate rheometer measurement, the shear banding observed in our LAOS study should be time-dependent associated with stress overshoots (Figure S1c), instead of steady shear banding.

An edge-induced disturbance could also persist in the bulk and lead to apparent shear banding.[25] However, the large aspect ratio of our confocal shear cell with A/H = 100 rules out edge instabilities as the origin of shear banding in our experiments. This conclusion is supported by our previous measurements on the penetration length of edge disturbance using the same setup and similar DNA solutions, where a penetration length of about 20H was found.[63]

A two-fluid model has also been proposed, which considers the coupling between shear flow and the fluctuation of polymer concentrations along the shear-gradient direction.[16−18,75] This model predicts a migration of polymer molecules under shear, which leads to a low polymer concentration and, therefore, low viscosity in the high-SRB. In both our previous study on spherical particles[65] and the present experiments on DNA-bridged dumbbells, we observe an enhanced diffusion of embedded tracers in the high-SRB (Figure 6), which confirms the low viscosity of the high-SRB microscopically from single particle dynamics. Although we do not directly measure the spatial variation of DNA concentrations, the observation of the fast particle dynamics in the high-SRB is consistent with the low polymer concentration predicted using the model.

However, the dynamics of embedded tracers in the high-SRB are spatially heterogeneous in the flow−vorticity plane. In our previous study on spherical particles, we showed that the number fraction of particles experiencing fast translational motion remains relatively low compared to particles exhibiting slow diffusive motion within the high-SRB.[65] The coexistence of fast and slow particles in the same shear band has been quantified further by dynamic heterogeneity in entangled DNA solutions. Similarly, in the current study, only a fraction of DNA-bridged dumbbells in the high-SRB exhibit strongly correlated enhanced translation and rotation with pronounced chain extension, while many other dumbbells show only weak

https://doi.org/10.1021/acs.macromol.0c02890
Macromolecules 2021, 54, 4186−4197

or no correlations and behave similar to those in the low-SRB. The strong abnormal dynamic heterogeneity implies shear-induced localized structures in the high-SRB. Such heterogeneity in the flow−vorticity plane has not been considered in the two-fluid model, where the polymer concentration is invariant normal to the shear gradient direction. For example, Cromer and co-workers imposed an initial concentration variation, $\phi = 1 + \delta \cos(\pi k y/H)$, where ϕ is the normalized polymer concentration, δ is the magnitude of the variation, and k is a wave number.[16,17] Accordingly, the steady-state concentration profile is only a function of y. As our experimental results indicate the presence of heterogeneity in the $x-z$ plane, it would be interesting to introduce concentration fluctuations along the flow and vorticity direction in an extended 3D two-fluid model and check how the growth and attenuation of in-plane concentration affect shear-banding flows.

Dynamic heterogeneity in the high-SRB suggests the formation of localized low-viscosity puddles within the background high-viscosity entangled polymer solutions. The positive correlation between the enhanced translation and the interparticle separation further indicates that these local puddles are characterized by strong chain stretching. Hence, we hypothesize that the low-viscosity puddles, which are present exclusively in the high SRB, originate microscopically from shear-induced chain stretching and alignment. This hypothesis is consistent with molecular dynamics simulations,[21,40−42] where the shear banding of entangled polymer fluids is associated with shear-induced local disentanglement of polymer networks in the high-SRB.[43]

5. CONCLUSIONS

In the present contribution, we synthesized DNA-bridged dumbbells by linking colloids with long λ-DNA molecules and studied their dynamics in sheared concentrated DNA solutions. The DNA solutions developed a clear shear-banding velocity profile at a high Weissenberg number. In the low-SRB, the orientation of the dumbbells exhibited a bimodal distribution with peaks along the flow and vorticity directions, whereas dumbbells in the high-SRB showed a preferential alignment along the flow direction. The difference in the orientational distributions indicated the change in the relative contributions of the normal stress differences and elastic stresses in the two coexisting bands. Furthermore, we found enhanced spatially heterogeneous translational and rotational dynamics of dumbbells in the high-SRB, which imply the formation of localized low-viscosity puddles. Positive correlations between the enhanced translational and rotational dynamics, as well as between the translational and rotational dynamics and the stretching of linking DNA chains, were found exclusively in the high-SRB. We compared our experimental findings with the existing competing mechanisms proposed for shear banding in entangled polymer fluids. We postulated that the localized low-viscosity puddles in the high-SRB arises from the shear-induced chain stretching and alignment, which lead to local disentanglement of polymer networks.

ASSOCIATED CONTENT

Supporting Information

The Supporting Information is available free of charge at https://pubs.acs.org/doi/10.1021/acs.macromol.0c02890.

More detailed information on reaction conditions/procedures and dumbbell tracking, additional rheological measurements of calf-thymus DNA solutions with and without particles, and derivation of relations between the MSD and direction-dependent diffusivities from Langevin equations (PDF)

Few dumbbells (circled) in the high-SRB exhibit faster translation and rotation during the same time interval. The video is played at 50× real time (AVI)

AUTHOR INFORMATION

Corresponding Authors

Kevin D. Dorfman − *Department of Chemical Engineering and Materials Science, University of Minnesota, Minneapolis, Minnesota 55455, United States;* orcid.org/0000-0003-0065-5157; Email: dorfman@umn.edu

Xiang Cheng − *Department of Chemical Engineering and Materials Science, University of Minnesota, Minneapolis, Minnesota 55455, United States;* orcid.org/0000-0002-2759-764X; Email: xcheng@umn.edu

Authors

Seunghwan Shin − *Department of Chemical Engineering and Materials Science, University of Minnesota, Minneapolis, Minnesota 55455, United States;* orcid.org/0000-0001-6581-1523

Yangming Kou − *Department of Chemical Engineering and Materials Science, University of Minnesota, Minneapolis, Minnesota 55455, United States;* orcid.org/0000-0002-9863-548X

Complete contact information is available at: https://pubs.acs.org/10.1021/acs.macromol.0c02890

Notes

The authors declare no competing financial interest.

ACKNOWLEDGMENTS

We thank Y. Qiao, X. Ma, P. Agrawal, H. Chuang, G. Richards, and W. Sweeney for help in preparation of DNA samples, D. Giles for sample characterizations, S. L. Biswal for discussion of DNA-bridged dumbbell synthesis, C. Macosko for discussion of sample characterization, and B. Leahy for discussion of anisotropic diffusivity. This work was supported by the NSF-CBET 1700771.

REFERENCES

(1) Olmsted, P. D. Perspectives on shear banding in complex fluids. *Rheol. Acta* **2008**, *47*, 283−300.

(2) Fielding, S. M. Shear banding in soft glassy materials. *Rep. Prog. Phys.* **2014**, *77*, 102601.

(3) Ovarlez, G.; Rodts, S.; Chateau, X.; Coussot, P. Phenomenology and physical origin of shear localization and shear banding in complex fluids. *Rheol. Acta* **2009**, *48*, 831−844.

(4) Schall, P.; van Hecke, M. Shear bands in matter with granularity. *Annu. Rev. Fluid. Mech.* **2010**, *42*, 67−88.

(5) McLeish, T. C. B.; Ball, R. C. A molecular approach to the spurt effect in polymer melt flow. *J. Polym. Sci., Polym. Phys.* **1986**, *24*, 1735−1745.

(6) Britton, M. M.; Callaghan, P. T. Nuclear magnetic resonance visualization of anomalous flow in cone-and-plate rheometry. *J. Rheol.* **1997**, *41*, 1365−1386.

(7) Callaghan, P. T.; Gil, A. M. Rheo-NMR of semidilute polyacrylamide in water. *Macromolecules* **2000**, *33*, 4116−4124.

(8) Tapadia, P.; Ravindranath, S.; Wang, S.-Q. Banding in entangled polymer fluids under oscillatory shearing. *Phys. Rev. Lett.* **2006**, *96*, 196001.
(9) Ravindranath, S.; Wang, S.-Q. Large amplitude oscillatory shear behavior of entangled polymer solutions: Particle tracking velocimetric investigation. *J. Rheol.* **2008**, *52*, 341−358.
(10) Boukany, P. E.; Wang, S.-Q. Shear banding or not in entangled DNA solutions depending on the level of entanglement. *J. Rheol.* **2009**, *53*, 73−83.
(11) Jaradat, S.; Harvey, M.; Waigh, T. A. Shear-banding in polyacrylamide solutions revealed via optical coherence tomography velocimetry. *Soft Matter* **2012**, *8*, 11677−11686.
(12) Sato, K.; Kunita, I.; Takikawa, Y.; Takeuchi, D.; Tanaka, Y.; Nakagaki, T.; Orihara, H. Direct observation of orientation distributions of actin filaments in a solution undergoing shear banding. *Soft Matter* **2017**, *13*, 2708−2716.
(13) Goudoulas, T. B.; Pan, S.; Germann, N. Double-stranded and single-stranded well-entangled DNA solutions under LAOS: A comprehensive study. *Polymer* **2018**, *140*, 240−254.
(14) Boukany, P. E.; Wang, S.-Q.; Ravindranath, S.; Lee, L. J. Shear banding in entangled polymers in the micron scale gap: a confocal-rheoscopic study. *Soft Matter* **2015**, *11*, 8058−8068.
(15) Germann, N. Shear banding in semidilute entangled polymer solutions. *Curr. Opin. Colloid Interface Sci.* **2019**, *39*, 1−10.
(16) Cromer, M.; Villet, M. C.; Fredrickson, G. H.; Leal, L. G. Shear banding in polymer solutions. *Phys. Fluids* **2013**, *25*, 051703.
(17) Cromer, M.; Fredrickson, G. H.; Leal, L. G. A study of shear banding in polymer solutions. *Phys. Fluids* **2014**, *26*, 063101.
(18) Peterson, J. D.; Cromer, M.; Fredrickson, G. H.; Gary Leal, L. Shear banding predictions for the two-fluid Rolie-Poly model. *J. Rheol.* **2016**, *60*, 927−951.
(19) Cromer, M.; Fredrickson, G. H.; Gary Leal, L. Concentration fluctuations in polymer solutions under mixed flow. *J. Rheol.* **2017**, *61*, 711−730.
(20) Wang, S.-Q.; Ravindranath, S.; Wang, Y.; Boukany, P. New theoretical considerations in polymer rheology: Elastic breakdown of chain entanglement network. *J. Chem. Phys.* **2007**, *127*, 064903.
(21) Mohagheghi, M.; Khomami, B. Molecular processes leading to shear banding in well entangled polymeric melts. *ACS Macro Lett.* **2015**, *4*, 684−688.
(22) Cao, J.; Likhtman, A. E. Shear banding in molecular dynamics of polymer melts. *Phys. Rev. Lett.* **2012**, *108*, 028302.
(23) Moorcroft, R. L.; Fielding, S. M. Criteria for shear banding in time-dependent flows of complex fluids. *Phys. Rev. Lett.* **2013**, *110*, 086001.
(24) Moorcroft, R. L.; Fielding, S. M. Shear banding in time-dependent flows of polymers and wormlike micelles. *J. Rheol.* **2014**, *58*, 103−147.
(25) Hemingway, E. J.; Fielding, S. M. Edge-induced shear banding in entangled polymeric fluids. *Phys. Rev. Lett.* **2018**, *120*, 138002.
(26) Hemingway, E. J.; Fielding, S. M. Edge fracture instability in sheared complex fluids: Onset criterion and possible mitigation strategy. *J. Rheol.* **2019**, *63*, 735−750.
(27) Walker, L. M. Rheology and structure of worm-like micelles. *Curr. Opin. Colloid Interface Sci.* **2001**, *6*, 451−456.
(28) Lerouge, S.; Berret, J.-F. Shear-induced transitions and instabilities in surfactant wormlike micelles. *Adv. Polym. Sci.* **2009**, *230*, 1−71.
(29) Boukany, P. E.; Wang, S.-Q. Use of particle-tracking velocimetry and flow birefringence to study nonlinear flow behavior of entangled wormlike micellar solution: From wall slip, bulk disentanglement to chain scission. *Macromolecules* **2008**, *41*, 1455−1464.
(30) Helgeson, M. E.; Reichert, M. D.; Hu, Y. T.; Wagner, N. J. Relating shear banding, structure, and phase behavior in wormlike micellar solutions. *Soft Matter* **2009**, *5*, 3858−3869.
(31) Calabrese, M. A.; Rogers, S. A.; Murphy, R. P.; Wagner, N. J. The rheology and microstructure of branched micelles under shear. *J. Rheol.* **2015**, *59*, 1299−1328.
(32) Calabrese, M. A.; Rogers, S. A.; Porcar, L.; Wagner, N. J. Understanding steady and dynamic shear banding in a model wormlike micellar solution. *J. Rheol.* **2016**, *60*, 1001−1017.
(33) Perkins, T.; Smith, D.; Chu, S. Direct observation of tube-like motion of a single polymer chain. *Science* **1994**, *264*, 819−822.
(34) Smith, D. E.; Perkins, T. T.; Chu, S. Self-diffusion of an entangled DNA molecule by reptation. *Phys. Rev. Lett.* **1995**, *75*, 4146−4149.
(35) Teixeira, R. E.; Dambal, A. K.; Richter, D. H.; Shaqfeh, E. S. G.; Chu, S. The individualistic dynamics of entangled DNA in solution. *Macromolecules* **2007**, *40*, 2461−2476.
(36) Schroeder, C. M. Single polymer dynamics for molecular rheology. *J. Rheol.* **2018**, *62*, 371−403.
(37) Zhou, Y.; Schroeder, C. M. Dynamically heterogeneous relaxation of entangled polymer chains. *Phys. Rev. Lett.* **2018**, *120*, 267801.
(38) Kirchenbuechler, I.; Guu, D.; Kurniawan, N. A.; Koenderink, G. H.; Lettinga, M. P. Direct visualization of flow-induced conformational transitions of single actin filaments in entangled solutions. *Nat. Commun.* **2014**, *5*, 5060.
(39) Carter, K. A.; Girkin, J. M.; Fielding, S. M. Shear banding in large amplitude oscillatory shear (LAOStrain and LAOStress) of polymers and wormlike micelles. *J. Rheol.* **2016**, *60*, 883−904.
(40) Mohagheghi, M.; Khomami, B. Elucidating the flow-microstructure coupling in the entangled polymer melts. Part I: Single chain dynamics in shear flow. *J. Rheol.* **2016**, *60*, 849−859.
(41) Mohagheghi, M.; Khomami, B. Elucidating the flow-microstructure coupling in entangled polymer melts. Part II: Molecular mechanism of shear banding. *J. Rheol.* **2016**, *60*, 861−872.
(42) Mohagheghi, M.; Khomami, B. Molecularly based criteria for shear banding in transient flow of entangled polymeric fluids. *Phys. Rev. E* **2016**, *93*, 062606.
(43) Wang, S.-Q. From Wall Slip to Bulk Shear Banding in Entangled Polymer Solutions. *Macromol. Chem. Phys.* **2019**, *220*, 1800327.
(44) van der Wel, C.; Bossert, N.; Mank, Q. J.; Winter, M. G. T.; Heinrich, D.; Kraft, D. J. Surfactant-free Colloidal Particles with Specific Binding Affinity. *Langmuir* **2017**, *33*, 9803−9810.
(45) Byrom, J.; Han, P.; Savory, M.; Biswal, S. L. Directing Assembly of DNA-Coated Colloids with Magnetic Fields To Generate Rigid, Semiflexible, and Flexible Chains. *Langmuir* **2014**, *30*, 9045−9052.
(46) Bhatia, S. R.; Russel, W. B. End-Capped Associative Polymer Chains between Nanospheres: Attractions in Ideal Solutions. *Macromolecules* **2000**, *33*, 5713−5720.
(47) Likos, C. N. Effective interactions in soft condensed matter physics. *Phys. Rep.* **2001**, *348*, 267−439.
(48) Schmatko, T.; Bozorgui, B.; Geerts, N.; Frenkel, D.; Eiser, E.; Poon, W. C. K. A finite-cluster phase in λ-DNA-coated colloids. *Soft Matter* **2007**, *3*, 703−706.
(49) Chambon, F.; Winter, H. H. Stopping of crosslinking reaction in a PDMS polymer at the gel point. *Polym. Bull.* **1985**, *13*, 499−503.
(50) Winter, H. H.; Chambon, F. Analysis of linear viscoelasticity of a crosslinking polymer at the gel point. *J. Rheol.* **1986**, *30*, 367−382.
(51) Kavanagh, G. M.; Ross-Murphy, S. B. Rheological characterization of polymer gels. *Prog. Polym. Sci.* **1998**, *23*, 533−562.
(52) Fried, M. G.; Bloomfield, V. A. DNA gelation in concentrated solutions. *Biopolymers* **1984**, *23*, 2141−2155.
(53) Kahn, J. S.; Hu, Y.; Willner, I. Stimuli-responsive DNA-based hydrogels: From basic principles to applications. *Acc. Chem. Res.* **2017**, *50*, 680−690.
(54) Miyoshi, E.; Nishinari, K. Non-Newtonian flow behaviour of gellan gum aqueous solutions. *Colloid Polym. Sci.* **1999**, *277*, 727−734.
(55) Lee, H.-C.; Brant, D. A. Rheology of concentrated isotropic and anisotropic xanthan solutions. 1. A rodlike low molecular weight sample. *Macromolecules* **2002**, *35*, 2212−2222.
(56) Dealy, J. M.; Tsang, W. K. W. Structural time dependency in the rheological behavior of molten polymers. *J. Appl. Polym. Sci.* **1981**, *26*, 1149−1158.

https://doi.org/10.1021/acs.macromol.0c02890
Macromolecules 2021, 54, 4186−4197

(57) Divoux, T.; Fardin, M. A.; Manneville, S.; Lerouge, S. Shear banding of complex fluids. *Annu. Rev. Fluid. Mech.* **2016**, *48*, 81.
(58) Fielding, S. M. Triggers and signatures of shear banding in steady and time-dependent flows. *J. Rheol.* **2016**, *60*, 821.
(59) Boudaghi-Khajehnobar, M.; Edwards, B. J.; Khomami, B. Effects of chain length and polydispersity on shear banding in simple shear flow of polymeric melts. *Soft Matter* **2020**, *16*, 6468−6483.
(60) Cheng, X.; McCoy, J. H.; Israelachvili, J. N.; Cohen, I. Imaging the microscopic structure of shear thinning and thickening colloidal suspensions. *Science* **2011**, *333*, 1276−1279.
(61) Lin, N. Y. C.; Goyal, S.; Cheng, X.; Zia, R. N.; Escobedo, F. A.; Cohen, I. Far-from-equilibrium sheared colloidal liquids: Disentangling relaxation, advection, and shear-induced diffusion. *Phys. Rev. E* **2013**, *88*, 062309.
(62) Lin, N. Y. C.; McCoy, J. H.; Cheng, X.; Leahy, B.; Israelachvili, J. N.; Cohen, I. A multi-axis confocal rheoscope for studying shear flow of structured fluids. *Rev. Sci. Instrum.* **2014**, *85*, 033905.
(63) Shin, S.; Dorfman, K. D.; Cheng, X. Effect of edge disturbance on shear banding in polymeric solutions. *J. Rheol.* **2018**, *62*, 1339−1345.
(64) Crocker, J. C.; Grier, D. G. Methods of digital video microscopy for colloidal studies. *J. Colloid Interface Sci.* **1996**, *179*, 298−310.
(65) Shin, S.; Dorfman, K. D.; Cheng, X. Shear-banding and superdiffusivity in entangled polymer solutions. *Phys. Rev. E* **2017**, *96*, 062503.
(66) Bartram, E.; Goldsmith, H. L.; Mason, S. G. Particle motions in non-Newtonian media. *Rheol. Acta* **1975**, *14*, 776−782.
(67) Iso, Y.; Koch, D. L.; Cohen, C. Orientation in simple shear flow of semi-dilute fiber suspensions 1. Weakly elastic fluids. *J. Non-Newt. Fluid* **1996**, *62*, 115−134.
(68) Hobbie, E. K.; Wang, H.; Kim, H.; Lin-Gibson, S.; Grulke, E. A. Orientation of carbon nanotubes in a sheared polymer melt. *Phys. Fluids* **2003**, *15*, 1196−1202.
(69) Leal, L. G. Slow motion of slender rod-like particles in 2nd order fluid. *J. Fluid Mech.* **1975**, *69*, 305−337.
(70) Gunes, D. Z.; Scirocco, R.; Mewis, J.; Vermant, J. Flow-induced orientation of non-spherical particles: Effect of aspect ratio and medium rheology. *J. Non-Newt. Fluid* **2008**, *155*, 39−50.
(71) Chen, D.; Semwogerere, D.; Sato, J.; Breedveld, V.; Weeks, E. R. Microscopic structural relaxation in a sheared supercooled colloidal liquid. *Phys. Rev. E* **2010**, *81*, 011403.
(72) Foister, R. T.; Ven, T. G. M. V. D. Diffusion of Brownian particles in shear flows. *J. Fluid Mech.* **1980**, *96*, 105−132.
(73) Takikawa, Y.; Orihara, H. Diffusion of Brownian Particles under Oscillatory Shear Flow. *J. Phys. Soc. Jpn.* **2012**, *81*, 124001.
(74) Leahy, B. D.; Cheng, X.; Ong, D. C.; Liddell-Watson, C.; Cohen, I. Enhancing rotational diffusion using oscillatory shear. *Phys. Rev. Lett.* **2013**, *110*, 228301.
(75) Burroughs, M. C.; Shetty, A. M.; Leal, L. G.; Helgeson, M. E. Coupled nonhomogeneous flows and flow-enhanced concentration fluctuations during startup shear of entangled polymer solutions. *Phys. Rev. Fluids* **2020**, *5*, 043301.

https://doi.org/10.1021/acs.macromol.0c02890
Macromolecules 2021, 54, 4186−4197